J3.4 Ensemble Kalman filter assimilation of Doppler radar data with a compressible nonhydrostatic model

Mingjing Tong and Ming Xue*
School of Meteorology and Center for Analysis and Prediction of Storms
University of Oklahoma, Norman, OK

1. Introduction

*Since its first introduction by Evensen (1994), the ensemble Kalman filter (EnKF) technique for data assimilation has received much attention. A number of studies have been done to exploit its applications and performances. The EnKF was designed to simplify the computation of the flow-dependent error statistics without the use of approximate closure scheme as extended Kalman filter does. Rather than solving the equation for the time evolution of the probability density function of the model state, EnKF applies the Monte Carlo method to estimate the forecast error statistics. A large ensemble of model states are integrated forward in time using the dynamic equations, the moments of the probability density function are then calculated from this ensemble of model states for different times (Evensen 2003).

In the recent decades, various techniques have been developed for analyzing and retrieving atmospheric state at the convective scale from Doppler radar data. These methods range from purely kinematic to expensive 4D variational method that employs a nonhydrostatic prediction model and its adjoint (e.g., Gal-Chen 1978; Sun *et al.* 1991; Qiu and Xu 1992; Shapiro *et al.* 1995; Sun and Crook 1997; Gao *et al.* 1999; Wu *et al.* 2000; Weygandt *et al.* 2002). Most of the latter work deals with retrieval and assimilation of radial velocity and/or reflectivity data from single Doppler radar. For the purpose of initializing NWP models, the 4DVAR method (e.g., Sun and Crook 1997; Gao *et al.* 1998) promises to provide an initial condition that is consistent with the prediction model and is able to effectively use multiple volume scans from radar. However, due to the need for an adjoint that should include detailed physics parameterizations and the high computational cost, 4DVAR assimilations of Doppler radar data have been limited to using relatively simple model configurations.

Compared to the 4DVAR method, the EnKF scheme is more flexible and much easier to set up. Under the right assumptions, its solution is equivalent to the optimal 4DVAR analysis. In fact, EnKF has recently been applied to the assimilation of simulated Doppler radar data for a convective storm (Snyder and Zhang 2003; Zhang *et al.* 2003) and of real radar data by Dowell *et al.* (2003). All three studies used the same anelastic cloud model of Sun and Crook (1997). Simple warm-rain microphysics scheme is used in these as well as afore-quoted 4DVAR studies with Wu et al (2000) being one exception. In the latter, the ice microphysics scheme used was simplified and microphysical variables, among others, were analyzed from dual-polarization radar data. In the study, water and ice phase microphysical variables are first derived from the polarization reflectivity data before being assimilated into the model.

In this study, we report on the development of an EnKF system based on a general-purpose compressible nonhydrostatic model, and the application of the system to the assimilation of simulated single Doppler radar radial velocity and/or reflectivity data. A sophisticated ice microphysics scheme is employed. The performance of the EnKF scheme in 'recovering' complete model structures, including wind, temperature, pressure fields and all water and ice categories are examined. The impact of radial velocity and reflectivity data as well as their spatial coverage on the analysis are investigated. Section 2 describes the EnKF assimilation system and design of OSS (Observing System Simulation) experiments, and section 3 present and discussed the experiment results. A concluding section is given at the end.

2. Assimilation System and Experimental Design

a) The prediction model and truth simulation

In this study, we test our EnKF assimilation system using simulated data from a classic May 20, 1977 Del City, Oklahoma supercell storm case (Ray *et al.* 1981). Such simulation experiments are commonly referred to as Observing System Simulation Experiments (OSSE, see, e.g., Lord *et al.* 1997). The forecast model used is the Advanced Regional Prediction System (ARPS; Xue *et al.* 2000), In this study, the ARPS is used in a 3D cloud model mode and the prognostic variables include three velocity components u, v, w, potential temperature θ, pressure p, and six categories of water substances (water vapor specific humidity q_v, cloud water mixing ratio q_c, rainwater mixing ratio q_r, cloud ice mixing ratio q_i, snow mixing ratio q_s and hail mixing ratio q_h). The microphysical processes are parameterized using the modified three-category ice scheme of Lin *et al.* (1983) and its implementation follows Tao and Simpson (1993).

For all experiments unless otherwise noted, the physical domain is $64km \times 64km \times 16km$. The model grid comprises of $35 \times 35 \times 35$ grid points, with grid intervals of 2 km in both x and y directions and of 0.5 km in the vertical. The truth simulation or nature run was initialized from a modified real sounding plus a $4K$ ellipsoidal thermal bubble centered at $x = 48km$, $y = 16km$ and $z = 1.5km$, and with radius of $10km$ in x and y and $1.5km$ in vertical directions. Open boundary conditions are used at the lateral

* Corresponding author address:
Dr. Ming Xue, SOM, SEC 1310, 100 E. Boyd,
Norman OK 73019,mxue@ou.edu.

boundaries. A radiation condition is also used at the top boundary. Free-slip conditions are applied to the bottom boundary. The length of simulation is 75 minutes. A constant wind of $u = 3$ ms^{-1} and $v = 14$ ms^{-1} is subtracted from the original sounding to keep the primary storm cell near the center of model grid. Despite a relatively coarse resolution, the evolution of the simulated storms is very similar to those documented in Xue *et al.* (2001).

b) Simulation of radar observations

The simulated observations are assumed to be available on the grid points. The radial velocity is calculated from

$$V_r = u\cos\alpha\sin\beta + v\cos\alpha\cos\beta + w\sin\alpha \quad , \tag{1}$$

where α is the elevation angle and β the azimuth angle of radar beams, and *u, v* and *w* are velocities from the simulation.

The logarithmic reflectivity is estimated from equations as follows:

$$dBZ = 10\log(Z) \, , \tag{2}$$

$$Z = Z_r + Z_s + Z_h \, , \tag{3}$$

where Z_r, Z_s, Z_h are contributions from rain, snow and hail. The rain component of the reflectivity is calculated from

$$Z_r = \frac{720C(\rho q_r)^{1.75}}{\pi^{1.75}(8.0\times10^6)^{0.75}\rho_r^{1.75}} \quad , \tag{4}$$

where *C* is a constant, $\rho_r = 1000kg/m^3$ is the density of rainwater, ρ is the density of air. If the temperature is less than zero centigrade then the snow component of reflectivity is

$$Z_s = \frac{720\,C\times0.176\rho_s^{0.25}(\rho q_s)^{1.75}}{0.93\pi^{1.75}(3\times10^6)^{0.75}\rho_i^{2}} \, , \tag{5}$$

otherwise ,

$$Z_s = \frac{720(\rho q_s)^{1.75}C}{\pi^{1.75}(3\times10^6)^{0.75}\rho_s^{1.75}} \, , \tag{6}$$

where $\rho_s = 100kg/m^3$ is the density of snow and $\rho_i = 917kg/m^3$ is the density of ice. The hail component is calculated from

$$Z_h = \left(\frac{720C}{(4.0\times10^4)^{0.75}\pi^{1.75}\rho_h^{1.75}}\right)^{0.95}(\rho q_h)^{1.6625} \, , \tag{7}$$

where $\rho_h = 913kg/m^3$ is the density of hail.

The radar is located at the southwest corner of the computational domain. For the data sampling and data assimilation, we assume the observation operator to be perfect. As with most 4DVAR and EnKF studies, the prediction model is also assumed perfect, i.e., no model error is explicitly taken into account.

c) The EnKF data assimilation procedure

Our EnKF implementation is based on the algorithm described by Evensen (1994), Burgers *et al.* (1998) and Houtekamer *et al.* (1998). The analysis equation is

$$x_i^a = x_i^f + P^f H^T[HP^f H^T + R]^{-1}(y_i^o - Hx_i^f) \, , \tag{8}$$

where *i* represents the *i*th ensemble member and x_i^f is the first guess obtained from the *i*th ensemble forecast. P^f is the forecast error covariance and R is the observation error covariance. Perturbed sets of observations are used to update each ensemble member and y_i^o is the *i*th perturbed observation. H is the observation operator, which converts the model states to the observation parameters. The forecast error covariances are calculated from

$$P^f H^T = \frac{1}{N-1}\sum_i^N (x_i^f - \overline{x^f})(Hx_i^f - \overline{Hx^f})^T \quad , \tag{9}$$

and

$$HP^f H^T = \frac{1}{N-1}\sum_i^N (Hx_i^f - \overline{Hx^f})(Hx_i^f - \overline{Hx^f})^T \, , \tag{10}$$

where the overbar denotes the ensemble mean and *N* is the number of ensemble members.

We start the initial ensemble forecast at the 20 minutes of the model simulated storm. To initialize the ensemble members, Gaussian noises with zero mean are added to the horizontally homogeneous initial guess that is based on the environmental sounding. The standard deviation of the random noises is 3 ms^{-1} for u , v and w and $3K$ for potential temperature. The pressure and moisture fields are not perturbed. The first analysis is performed at 25 minutes. One hundred ensemble members are used for the assimilation experiments.

The observations are assimilated every 5 minutes. The observation errors are assumed to be uncorrelated; therefore, observations can be and are analyzed sequentially one at a time. We limit the influence region of each observation to a rectangular region with half width of 2 grid intervals in both horizontal and vertical directions, a procedure known as covariance localization. Observations are perturbed by adding Gaussian noises, with the standard deviations being 1 ms^{-1} for radial velocity and 5 dBZ for reflectivity.

Table 1 gives a list of ten experiments reported in this paper. First the assimilation scheme is tested by only assimilating the simulated radial velocity data with full data coverage or data covering regions with significant reflectivity only. The impact of using reflectivity data is evaluated among other experiments.

3. The Assimilation Experiments

a) Assimilations using radial velocity data only

In experiment VrFull we assume that the radial velocity data cover the entire computational domain. In experiment VrCloudy the same data are available only in cloudy regions where reflectivity is greater than 10dBZ. Although in real cases, the radial velocity data are generally unavailable or are unreliable outside the cloudy regions, we would like to see how data coverage impacts the quality of EnKF assimilation.

Table 1. List of Data Assimilation Experiments

Experiment	Observation: Radial velocity (Vr) and/or Reflectivity (Z)	Update pressure	Update q_i, q_s, q_h	Update u, v, w, q_v, q_c, q_i when assimilating reflectivity
VrFull	Vr	yes	yes	
VrFLD	The same as VrFull, except for a 2.5 times as large a domain in the y direction			
VrCloudy	Vr (Z > 10 dBZ)	yes	yes	
VrCnop	Vr (Z > 10 dBZ)	no	yes	
ZCloudy	Z (Z > 10 dBZ)	no	yes	yes
VrZCa	Vr & Z (Z > 10 dBZ)	no	yes	yes
VrZCb	Vr & Z (Z > 10 dBZ)	no	yes	no
VrZCc	Vr & Z (Z > 10 dBZ)	no	yes	yes, start from 4th cycle
VrCZfull	Vr (Z > 10dBZ) & Z	no	yes	yes, start from 4th cycle
VrCnoice	Vr (Z > 10 dBZ)	no	no	

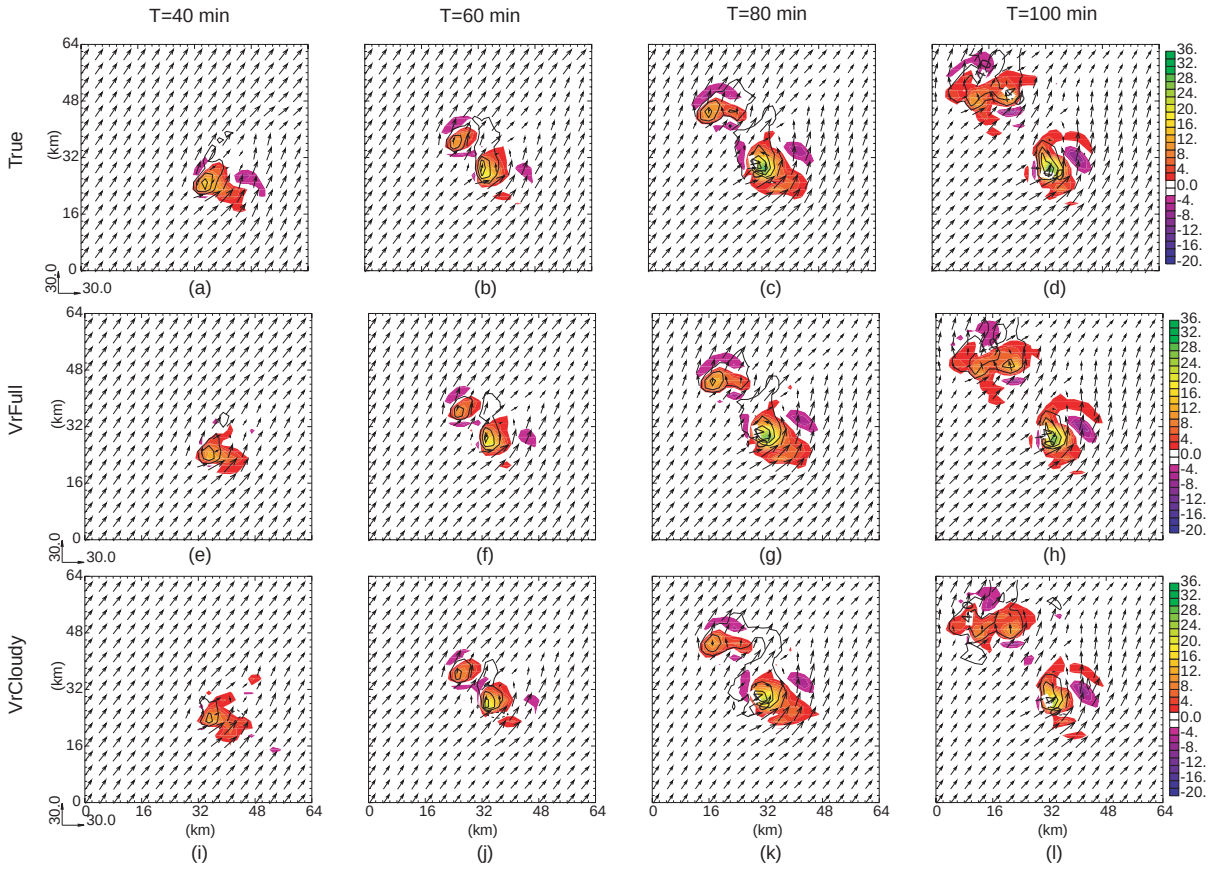

Figure 1. Vertical velocity (m s^{-1}; shaded), horizontal wind vectors (m s^{-1}), and perturbation potential temperature θ' (K; contour) at z=6 km for truth simulation (a)~(d), experiments VrFull (e)~(h) and VrCloudy (i)~(l) at T=40, 60, 80 and 100 min.

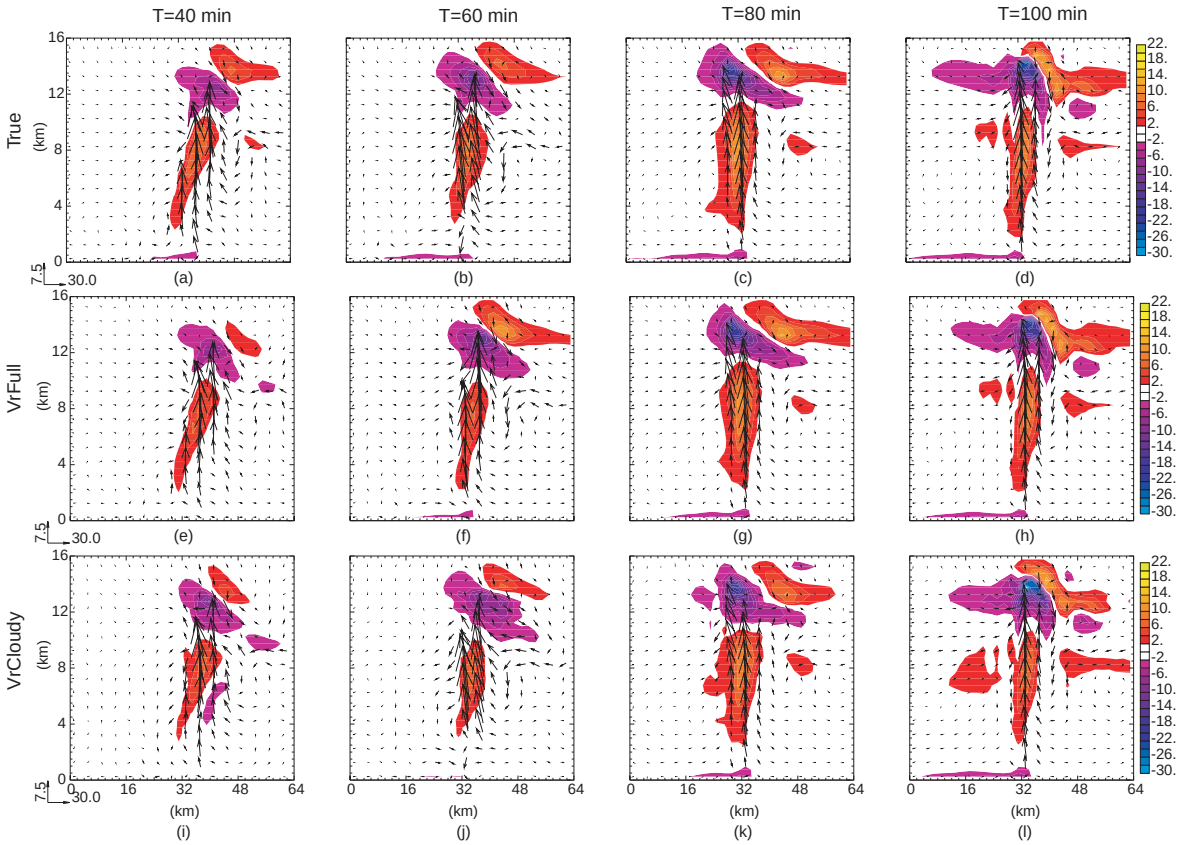

Figure 2. The vertical cross-sections of wind vectors (m s^{-1}), perturbation potential temperature (K; shaded), which pass through the maximum updraft, for the truth simulation (a)~(d), experiment VrFull (e)~(h) and experiment VrCloudy (i)~(l) at T=40, 60, 80 and 100 min.

As one can see by comparing with the truth fields, the wind, temperature, and microphysical variable fields can be accurately retrieved by experiment VrFull (Figs. 1, 2, 10). At 80 minutes (the end of 12th assimilation cycle), the maximum updraft is 40.5 ms^{-1}, which is very close to the 40.7 ms^{-1} of truth simulation (Fig. 2 though the specific maximum values are not shown). The strength of the low level cold pool, represented by the minimum perturbation potential temperature at the first scalar level (250m) above ground, is -5.42 K for the simulation and -5.0 K for experiment VrFull (not shown). The overall structure and evolution of the assimilated storm is very close to the true storm at this stage, indicating that the assimilation of radial velocity data using the EnKF scheme is successful.

Compared to VrFull, VrCloudy is also able to establish the basic structures of the model storm well. The evolution of the model storm, including the cell splitting between 40 and 60 minutes and further splitting after 80 minutes are all well reproduced (Fig. 1). However, the strength of the updraft, the edge and strength of the low level cold pool (not shown) and also the distribution of the six water substances are not as accurate as in VrFull (Figs. 1, 2 and 10). Since we added perturbations to the initial guess everywhere and covariance localization was made, the environmental state in the clear air regions can not be updated by the analysis directly when data are limited to the cloudy regions. The model fields are therefore somewhat noisy. In real cases, other data representative of the environment can be used to improve the environmental analysis.

We use the *rms* error of the mean of ensemble analyses and forecasts to judge the quality of the mean analysis. The *rms* errors are averaged over those grid points where the reflectivity is greater than 10 dBZ. The errors for VrFull and VrCloudy are plotted in Fig. 3. The *rms* errors of velocities, temperature and hydrometeor variables are seen to decrease rapidly in the first four assimilation cycles (over 20 minutes). The *rms* errors are much smaller when the data covers the entire domain.

The EnKF data assimilation scheme works well for all, except pressure fields. Figure 3(e) shows that for the case when pressure field is analyzed (updated by the analysis), the pressure field becomes less accurate than the background forecast after each analysis. In fact, in this case and for almost all cycles, it is the model forecast that reduces the error in pressure. When data coverage is limited to the cloudy regions, the situation becomes even worse (the red curve in Fig. 3 (e)). The model pressure field (not shown here) indicates excessive acoustic oscillations in the analysis and forecast solutions, especially at

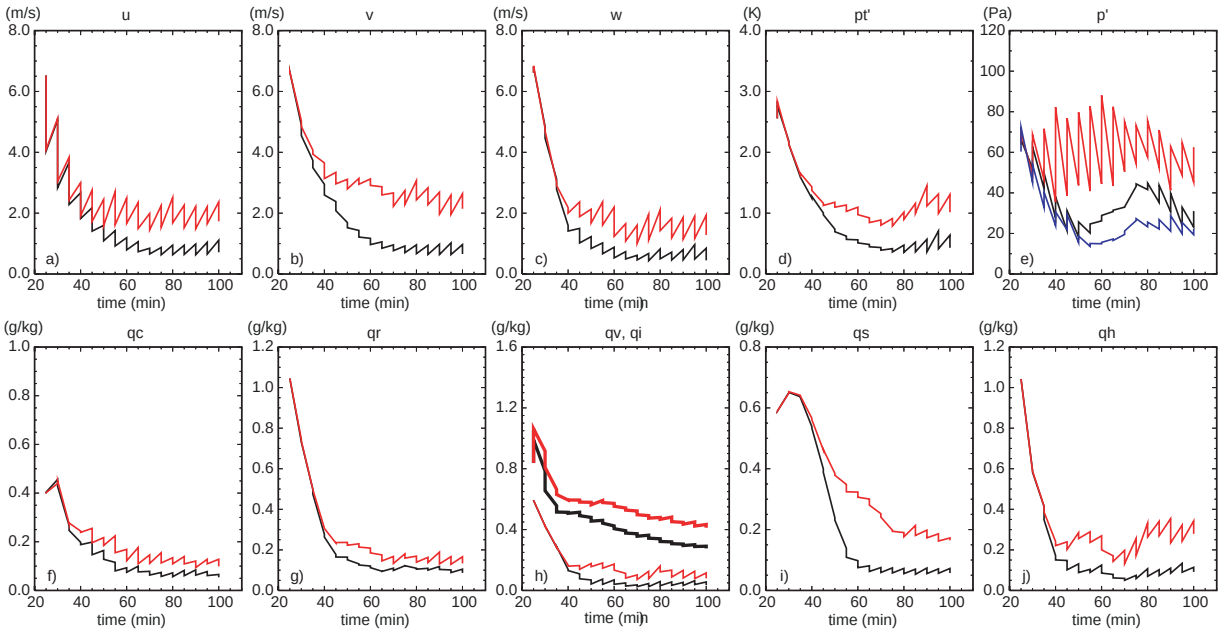

Figure 3. The rms errors of the mean of ensemble forecasts and analyses, averaged over points at which the reflectivity is greater than 10dBZ for: a) u (ms^{-1}), b) v (ms^{-1}), c) w (ms^{-1}) and d) perturbation potential temperature θ' (K), e) perturbation pressure p' (Pa), f) q_c (g kg^{-1}) g) q_r (g kg^{-1}), h) q_v (g kg^{-1}; thick curve), q_i (g kg^{-1}), i) q_s (g kg^{-1}), j) q_h (g kg^{-1}), for experiment VrCloudy (red), experiment VrFull (black) and experiment VrFLD (only the rms error of p' is shown, which is the blue curve in (e)).

the lower levels. The problem results from the compressible nature of the forecast model. Because the background error correlations associated with the acoustic modes cannot be reliably estimated (mainly because of its high frequency), it is hard for the analysis to exactly satisfy the mass continuity equation.

When the continuity equation is not satisfied, acoustic modes get excited. The problem is more severe during the earlier assimilation cycles and/or when data coverage is incomplete. The acoustic wave amplitudes actually decreases in the subsequent model forecast, due to dynamic adjustment and built-in damping of acoustic modes in the model. When the data coverage is complete, it takes only a few cycles for the pressure field to adjust and become close to the truth, except in the lower layer. The situation is worse when data coverage is incomplete because in the clear air regions, the model variables are not updated by the analysis and large imbalances occur at the edge of cloudy regions, large amplitude acoustic waves are excited there. As a result, the forecast error covariance computed from the ensemble states becomes incorrect and the analysis update does not improve the background forecast of pressure. In the cloud-scale EnKF assimilation studies that use an anelastic model, pressure is diagnosed from the wind field. When wind field does not satisfy the anelastic mass continuity equation, similar problem may occur although this issue has not been discussed in the literature.

The open lateral boundary condition used in our simulations is another possible source of mass continuity error. To examine the boundary effect, another experiment VrFLD is performed that is the same as VrFull, except the domain 2.5 times as long in the y direction. As the lateral boundaries are further removed from the storms, the pressure analysis and forecast errors are significantly reduced (as shown by the blue curve in Fig 3 b).

Since the analysis update to pressure generally hurts the model solution, the update to pressure should not be performed. This is so in our later experiments, and in general, the model is able to establish a pressure field that is consistent with the wind and other fields.

b) Impact of assimilating reflectivity data

Reflectivity is a measurement that is provided by all types of weather radar. In this section, we examine if reflectivity data alone is sufficient for the model to reproduce the true storm, and we also study its value when used in combination with radial velocity data (which is unavailable from non-Doppler radars). We note that the observation operator for reflectivity is nonlinear and there exist more uncertainties in the operator with reflectivity data than with radial velocity. In our model with ice microphysics, the rainwater, snow and hail mixing ratios, q_r, q_s, and q_h, are directly related to the reflectivity (Eqs. 3-6). The experiments therefore further test the performance of EnKF scheme in the case of nonlinear observation operator. In the first experiment ZCloudy, only simulated reflectivity greater than 10dBZ is assimilated.

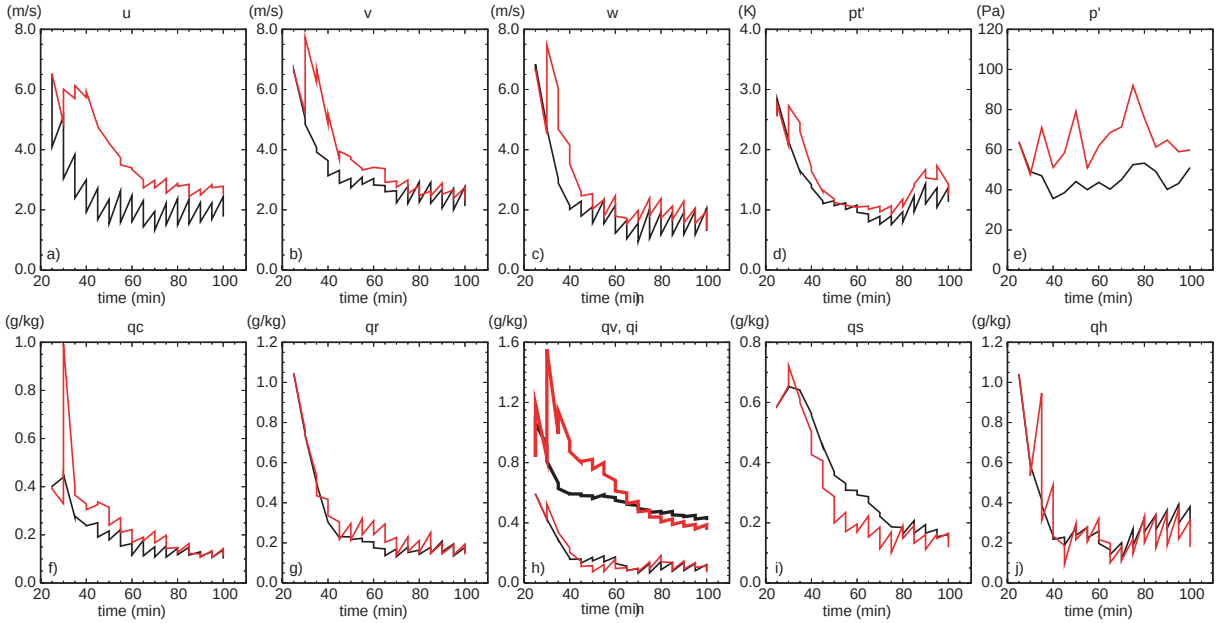

Figure 4. The rms errors of the mean of ensemble forecasts and analyses, averaged over points at which the reflectivity is greater than 10dBZ for: a) u (ms^{-1}), b) v (ms^{-1}), c) w (ms^{-1}) and d) perturbation potential temperature θ' (K), e) perturbation pressure p' (Pa), f) q_c (g kg^{-1}) g) q_r (g kg^{-1}), h) q_v (g kg^{-1}; thick curve), q_i (g kg^{-1}), i) q_s (g kg^{-1}), j) q_h (g kg^{-1}),for experiments ZCloudy (red) and VrCnop (black).

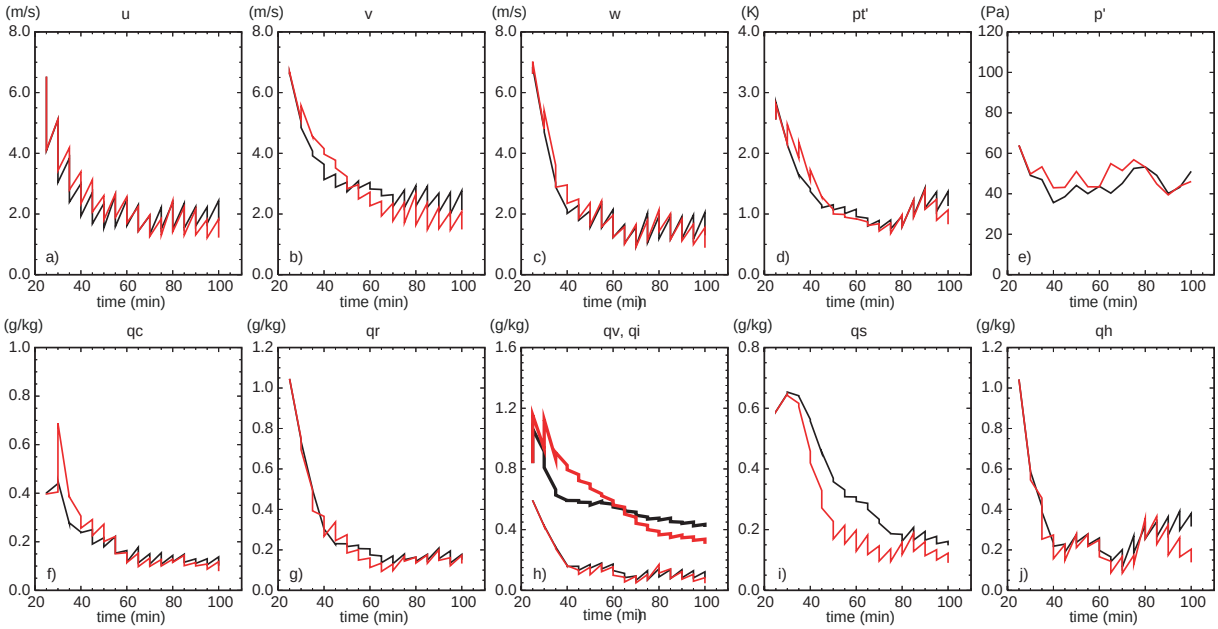

Figure 5. As Fig. 4 for experiments VrCnop (black) and VrZCa (red).

As can be seen in Fig. 4 (red curves), the analysis starts to reduce the *rms* errors for q_r and q_h first (starting from the second cycle) and then for w, θ', q_c, q_v, q_s and q_i. Significant reduction in u and v errors did not start until after six to seven cycles. We compare this experiment with VrCnop, which is the same as VrCloudy, except that the pressure field is not updated. The accuracy of the retrieved snow and hail fields is better while the accuracy of retrieved rain and ice fields is comparable. For water vapor field, the rms error is smaller than that of VrCnop in the later part of the analysis period. But the velocity and temperature fields are not as good as those of VrCnop. The result is reasonable, because the relation between reflectivity and the wind and temperature fields is indirect. The information of reflectivity can be used to effectively correct errors in

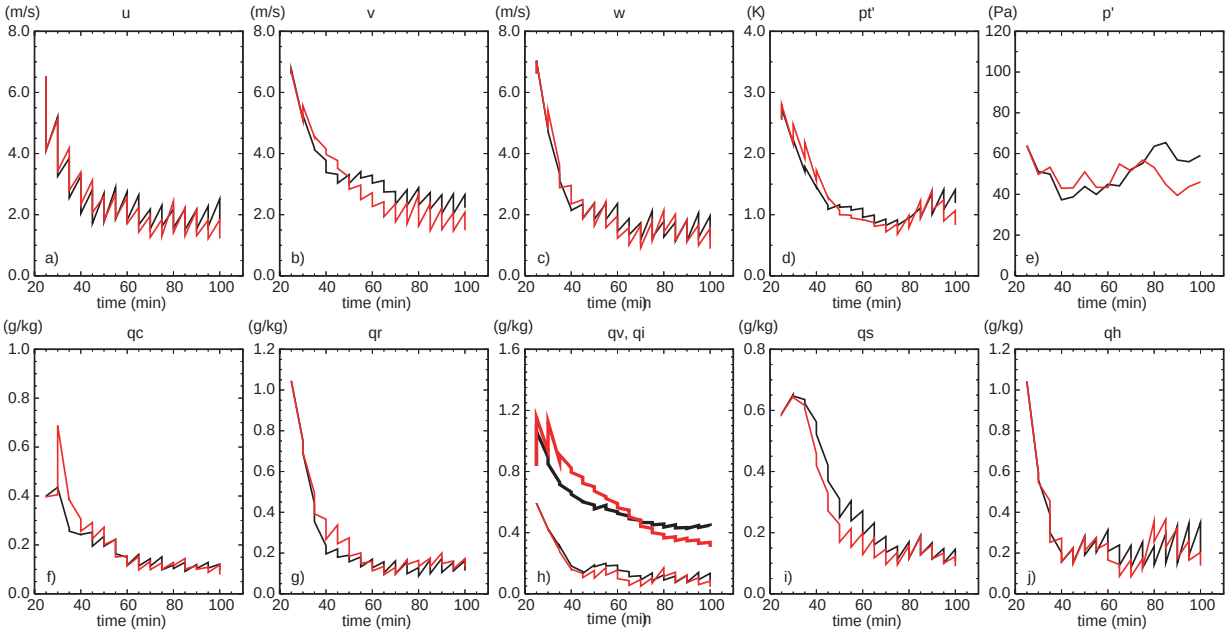

Figure 6. As Fig. 4 but for experiments VrZCa (red) and VrZCb (black).

the wind and temperature fields only after the EnKF system produces correct forecast error covariances between the variables.

In the next set of experiments, we combine the radial velocity and the reflectivity data into the assimilation process. In experiment VrZCa, both the radial velocity and reflectivity in cloudy regions are assimilated (red curve in Fig. 5). Compared to VrCnop, we can see that when additional reflectivity data are assimilated the analysis errors of q_s, q_h, q_r and q_i are smaller than those in VrCnop. Whereas for most of the other control variables, in the first part of assimilation period (before 65 min), including reflectivity data hurts the model solution. In the later part of the period, the analysis update of all variables, except pressure, is better or is as good as in VrCnop. Our explanation is that at the early stage of the assimilation period, background error covariances between reflectivity and the fields not directly related to reflectivity were not reliable. Updating these variables based on reflectivity data and the unreliable covariances therefore hurts the analysis. As the model state gets closer to truth, the covariances estimated are improved, leading to direct positive impact on other fields.

We note that in Dowell *et al.* (2003) that uses warm rain microphysics, only q_r is updated when assimilating reflectivity observations. We performed a corresponding experiment, VrZCb, in which only q_r, q_s, and q_h were updated when assimilating reflectivity (black curve in Fig. 6). With respect to the wind and temperature fields, this does lead to better results before the sixth cycle. However, after the sixth cycle, the accuracy of the wind and temperature fields is not as good as the case that we do update all variables (except for pressure). As discussed earlier, in the EnKF system, there is clearly a delay before reliable covariances between reflectivity and the wind and thermodynamic fields are established. After the initial delay, the reflectivity becomes directly beneficial in retrieving the wind and thermodynamic fields and the assimilation of it leads to overall better analysis. For this reason, we do not believe it appropriate to exclude wind and temperature from the analysis update based on reflectivity data.

To see if we can further improve the analysis, in VrZCc we apply the update due to reflectivity to q_r, q_s, and q_h only before the fourth cycle. After the fourth cycle, all control variables (except for pressure) are updated based on reflectivity. Figure 7 shows that by doing so, the analyses for all control variables are improved and so is the forecast of pressure field.

In the previous experiments, only reflectivity larger than 10 dBZ is assimilated. In reality, zero reflectivity outside the cloudy regions also contains valid information. One can assume that the assimilate reflectivity data cover the entire analysis domain. In our next OSS experiment, named VrCZfull, such assumption is made, but radial velocity data are still only available in cloudy regions (Z > 10 dBZ). As was done in experiment VrZCc, the velocities (*u, v, w*), perturbation potential temperature θ', q_v, q_c, and q_i are updated starting from the fourth cycle when assimilating reflectivity. Figure 8 shows that with the complete reflectivity coverage, not only the microphysical fields are much improved, but also the wind and temperature fields. The complete coverage of reflectivity data can remove spurious disturbance that can otherwise develop in the data void regions. Experiment VrCZfull produces the best result among those that does not assume complete coverage of V_r data.

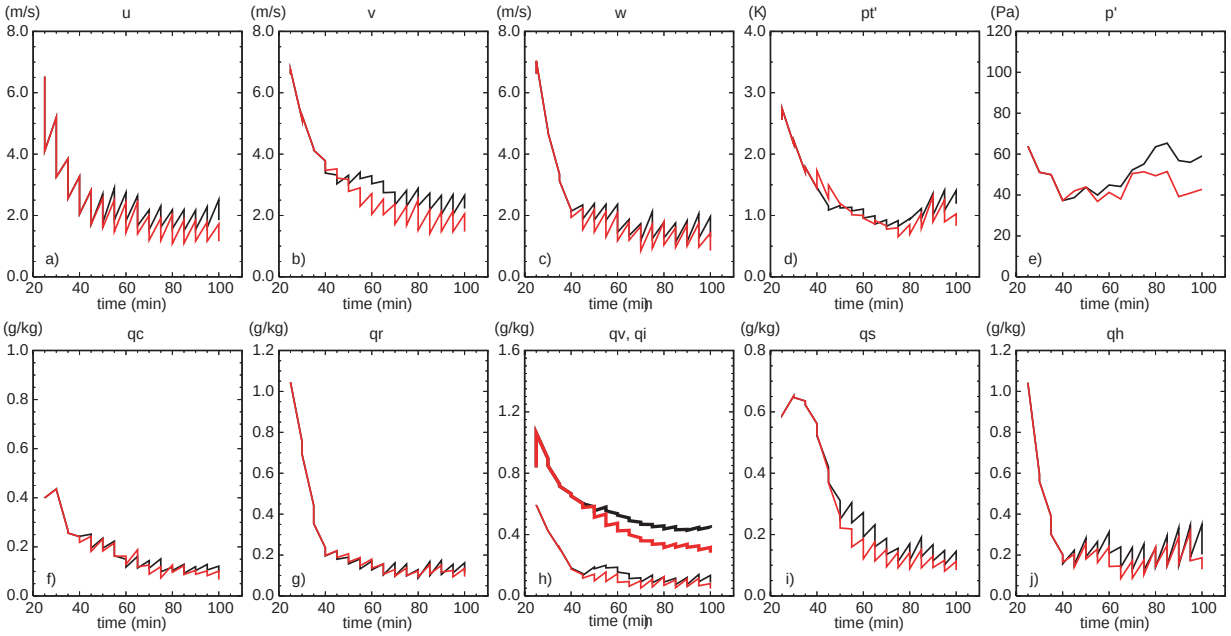

Figure 7. As Fig. 4 but for experiments VrZCb (black) and VrZCc (red).

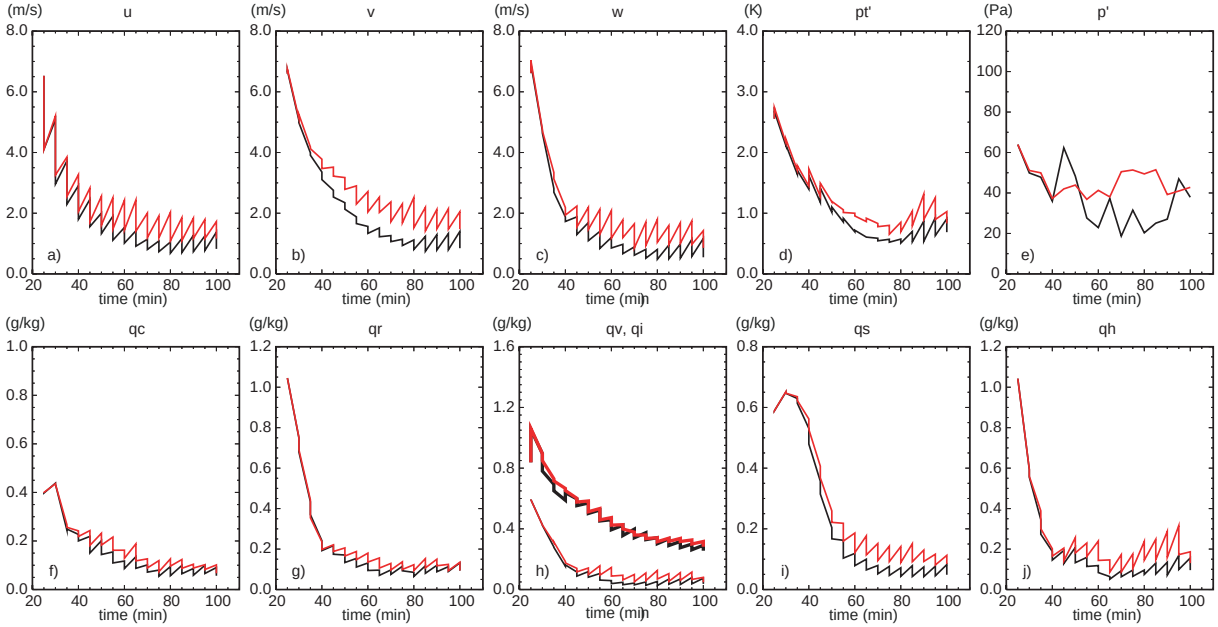

Figure 8. As Fig. 4 but for experiments VrZCc (red) and VrCZfull (black).

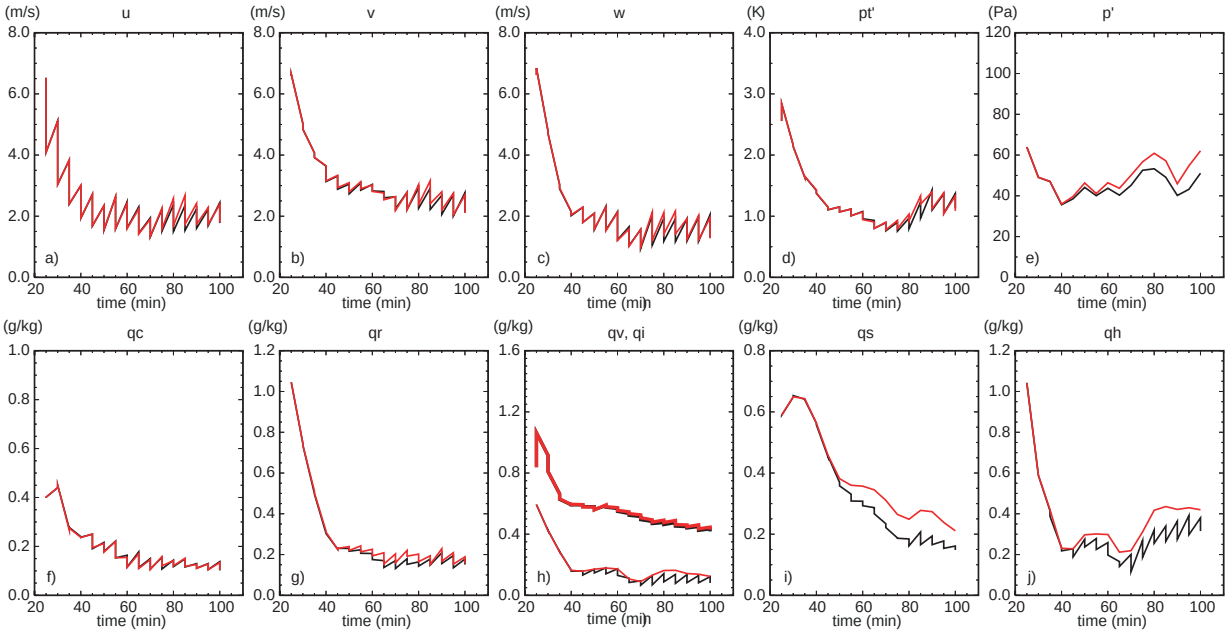

Figure 9. As Fig. 4 but for experiments VrCnop (black) and VrCnoice (red).

c) Retrieval of microphysical fields

The microphysics retrieval is an important aspect of convective-scale data assimilation. Relatively few previous studies have focused on this problem. Most of these studies used only simple microphysical parameterization and the ice phase is usually excluded. The recent attempt of Wu et al (2000) uses a 4DVAR data assimilation system to assimilate dual-polarization radar data into a model of deep convective cloud with both liquid and ice phase microphysics. In their study, the microphysics scheme is simplified and consists of only three categories: rain, hail and cloud liquid-ice. The reflectivity and differential reflectivity data were converted to rain and hail mixing ratios first, rather than being directly assimilated. The differential reflectivity data were necessary for such a conversion. In our study, the original detailed ice microphysics parameterization is used and only regular reflectivity measurement is assumed available. Our problem is more difficult here because more water and ice species have to be determined and no dual polarization information is available. Figure 10 shows the distribution of the five categories of hydrometeor for the true run and for assimilation experiments VrFull, VrCnop, VrCnoice, ZCloudy and VrCZfull. The figure shows that the EnKF data assimilation system is able to establish detailed microphysical structures that have very good fidelity. The quality of actual analysis does depend on the usage and availability of data, as seen earlier by the error plots.

To better understand the way the EnKF scheme works when retrieving the microphysical fields, we performed another experiment, named VrCnoice, in which q_i, q_s, and q_h (as well as pressure) are not updated by the analysis and only radial velocity in cloudy regions are assimilated. For these three variables, the difference between VrCnoice and VrCnop is relatively small before the 6th cycle, but becomes significant after that time (Fig. 9). For the early period, the relatively small difference reflects relatively weak or unreliable link (through background error covariance) between the observation (V_r) and these three variables. The link apparently becomes stronger and more effective in correcting errors in these fields at the later stage. On the other hand, despite of the lack of direct correction to q_i, q_s, and q_h by V_r, the errors in the former are still reduced in time in general. Such reductions are achieved through model dynamics – when other model fields are improved, fields that are not directly updated have to adjust and become consistent with these other fields. The more accurate hydrometeor fields, in turn, help improve the overall model state. The link through model dynamics is more important at the early period of assimilation when background error covariances are less reliable.

Despite the effectiveness of radial velocity assimilation, the reflectivity is most important for retrieving the microphysical fields because it has the most direct link to the hydrometeors. Experiment ZCloudy helps us understand this point. With only reflectivity, we cannot obtain as good an analysis for wind and thermodynamic fields, but the microphysical fields can be retrieved accurately (Fig. 4 and Fig. 10).

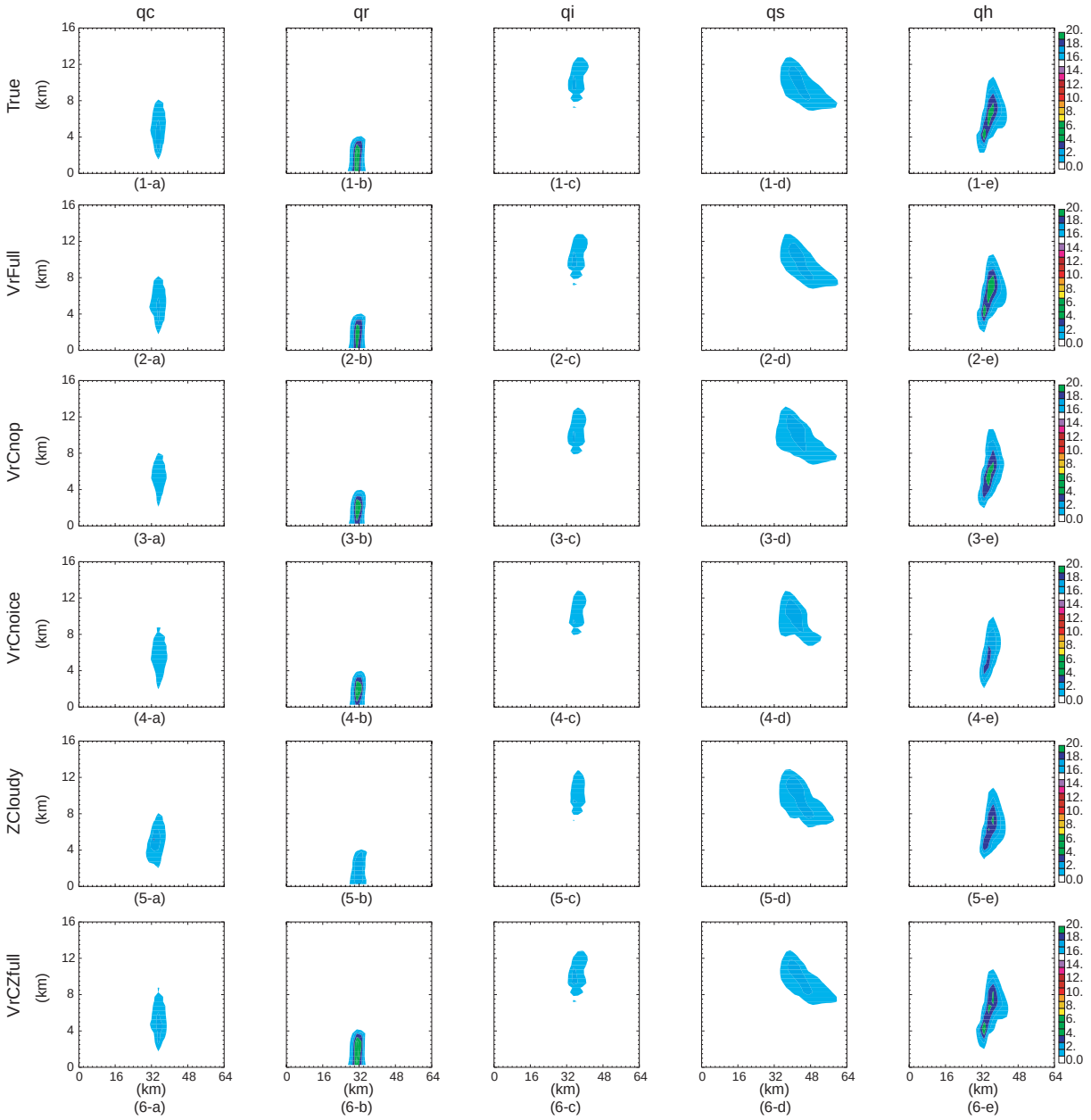

Figure 10. The cross-sections of q_c, q_r, q_i, q_s and q_h (g kg^{-1}) fields that pass through the maximum updraft for the truth simulation (1-a)~(1-e), and experiments VrFull (2-a)~(2-e), VrCnop (3-a)~(3-e), VrCnoice (4-a)~(4-e), ZCloudy (5-a)~(5-e) and VrCZfull (6-a)~(6-e) at T=65 min.

4. Concluding and Discussion

In this study we applied the ensemble Kalman filter technique to the assimilation of simulated radar radial velocity and reflectivity data using a compressible model with a complex microphysics scheme. The method is shown to have great potentials for the assimilation of such data. Through flow-dependent forecast error covariance estimation from the ensemble states, not only the wind and thermodynamic fields can be retrieved accurately, all five categories of hydrometeor can also be retrieved successfully. Reliable covariances between the observations and variables not directly related to them can be obtained after a few assimilation cycles even when they are started from initial guess made of an environmental sounding plus random perturbations. After the initial number of cycles, useful observational information can be spread to the indirectly related variables through reliable forecast error covariances. Updating indirectly related variables after the first few cycles when assimilating reflectivity data produces the best

analysis. Using reflectivity information in clear air regions is also beneficial. When using a compressible model, acoustic wave mode can be excited by errors in the wind and pressure analyses and it is recommended that pressure be excluded from the analysis update. This choice is shown to work the best.

Of course, caution should be applied when interpreting OSSE results. Both forecast model and forward observation operators are assumed perfect, which happens to work well for OSSE data. Despite a recent success in applying EnKF to real radar data (which still used a model in idealized settings), much work is still needed in moving us in the direction of real case and real data.

Acknowledgement

This work was supported by NSF grant ATM0129892. The second author was also supported by NSF ATM9909007 and an DOT-FAA grant.

Reference

Burgers, G., P. J. van Leeuwen, and G. Evensen, 1998: Analysis scheme in the ensemble Kalman filter. *Mon. Wea. Rev.*, **126**, 1719-1724.

Dowell, D., and F. Zhang, 2003: Wind and Thermodynamic Retrievals in the 17 May 1981 Arcadia, Oklahoma Supercell: Ensemble Kalman Filter Experiments. Submitted to *Mon. Wea. Rev*.

Evensen, G., 1994: Sequential data assimilation with a nonlinear quasi-geostrophic model using Monte Carlo methods to forecast error statistics. *J. Geophys. Res.*, **99** (C5), 10 143-10 162.

Evensen, G., 2003: The ensemble Kalman filter: Theoretical formulation and practical implementation. Submitted to *Ocear Dynamics*.

Gal-Chen, T., 1978: A method for the initialization of the anelastic equations: Implications for matching models with observations. *Mon. Wea. Rev.*, **106,** 587-606.

Gao, J., M. Xue, Z. Wang, and K. K. Droegemeier, 1998: The initial condition and explicit prediction of convection using ARPS adjoint and other retrievals methods with WSR-88D data. *12th Conf. Num. Wea. Pred.*, Phoenix AZ, Amer. Meteor. Soc., 176-178.

Gao, J.-D., M. Xue, A. Shapiro, and K. K. Droegemeier, 1999: A variational method for the analysis of three-dimensional wind fields from two Doppler radars. *Mon. Wea. Rev.*, **127,** 2128-2142.

Houtekamer, P. L., and H. L. Mitchell, 1998: Data assimilation using an ensemble Kalman filter technique. *Mon. Wea. Rev.*, **126**, 796-811.

Lord, S. J., E. Kalnay, R. Daley, G. D. Emmitt, and R. Atlas, 1997: Using OSSEs in the design of the future generation of integrated observing systems. *Preprint volume, 1st Symposium on Integrated Observation Systems*, Long Beach, CA, Amer. Meteor. Soc.

Qiu, C.-J. and Q. Xu, 1992: A simple adjoint method of wind analysis for single-Doppler data. *J. Atmos. Oceanic Technol.*, **9,** 588-598.

Ray, P. S., B. Johnson, K. W. Johnson, J. S. Bradberry, J. J. Stephens, K. K. Wagner, R. B. Wilhelmson, and J. B. Klemp, 1981: The morphology of severe tornadic storms on 20 May 1977. *J. Atmos. Sci.*, **38,** 1643-1663.

Shapiro, A., S. Ellis, and J. Shaw, 1995: Single-Doppler radar retrievals with Phoenix II data: Clear air and microburst wind retrievals in the planetary boundary layer. *J. Atmos. Sci.*, **52,** 1265-1287.

Snyder, C., and F. Zhang, 2003: Assimilation of Simulated Doppler Radar Observations with an Ensemble Kalman Filter. *Mon. Wea. Rev.*, **131**, 1663-1677.

Sun, J., D. W. Flicker, and D. K. Lilly, 1991: Recovery of three-dimensional wind and temperature fields from simulated single-Doppler radar data. *J. Atmos. Sci.*, **48,** 876-890.

Sun, J. and N. A. Crook, 1997: Dynamical and microphysical retrieval from Doppler radar observations using a cloud model and its adjoint. Part I: Model development and simulated data experiments. *J. Atmos. Sci.*, **54,** 1642-1661.

Weygandt, S. S., A. Shapiro, and K. K. Droegemeier, 2002: Retrieval of Model Initial Fields from Single-Doppler Observations of a Supercell Thunderstorm. Part I: Single-Doppler Velocity Retrieval. *Mon. Wea. Rev.*, **130,** 433-453.

Wu, B., J Verlinde., and J. Sun, 2000: Dynamical and Microphysical retrievals from Doppler Radar observations of a deep convective cloud. *J. Atmos. Sci.*, 57, 262-283.

Xue, M., K. K. Droegemeier, and V. Wong, 2000: The Advanced Regional Prediction System (ARPS) - A multiscale nonhydrostatic atmospheric simulation and prediction tool. Part I: Model dynamics and verification. *Meteor. Atmos. Physics*, **75,** 161-193.

Xue, M., K. K. Droegemeier, V. Wong, A. Shapiro, K. Brewster, F. Carr, D. Weber, Y. Liu, and D. Wang, 2001: The Advanced Regional Prediction System (ARPS) - A multi-scale nonhydrostatic atmospheric simulation and prediction tool. Part II: Model physics and applications. *Meteor. Atmos. Phys.*, **76,** 143-166.

Zhang, F., C. Snyder, and J. Sun, 2003: Impacts of initial estimate and observations on the convective-scale data assimilation with an ensemble Kalman filter. Submitted to *Mon. Wea. Rev.*